Electronic Supplementary Material (ESI) for CrystEngComm.

Structural distortions in the high-pressure polar phases of ammonium metal formates

Supporting Information

Ines E. Collings[1*], Maxim Bykov[2], Elena Bykova[2], Matthew G. Tucker[3], Sylvain Petitgirard[2], Michael Hanfland[4], Konstantin Glazyrin[5], Sander van Smaalen[1], Andrew L. Goodwin[6], Leonid Dubrovinsky[2], Natalia Dubrovinskaia[1]

[1]Laboratory of Crystallography, University of Bayreuth, D-95440 Bayreuth, Germany.
[2]Bayerisches Geoinstitut, University of Bayreuth, D-95440 Bayreuth, Germany.
[3]Oak Ridge National Laboratory, Tennessee, USA.
[4]European Synchrotron Radiation Facility, BP 220, 38043 Grenoble, Cedex 9, France.
[5]Deutsches Elektronen-Synchrotron DESY, Notkestrasse 85, D-22603 Hamburg, Germany.
[6]Inorganic Chemistry Laboratory, Department of Chemistry, University of Oxford, South Parks Road, Oxford OX1 3QR, UK.
*Author to whom correspondence should be addressed;
E-mail: ines.collings@uni-bayreuth.de

Contents

1 SCXRD of $[NH_4][Ni(HCOO)_3]$

Room temperature and 100 K single-crystal X-ray diffraction (SCXRD) measurements were performed on $[NH_4][Ni(HCOO)_3]$ using a MAR345 dtb diffractometer equipped with a rotating anode generator of Mo-Kα radiation. ϕ scans were measured at steps of 1° for a full 360° rotation. Crystallographic details on the data collection and refinement are given in Table S1. Figure S1 shows the refined crystal structures of $[NH_4][Ni(HCOO)_3]$ at 293 K and 100 K where the ammonium cations are observed to be split in two positions for the low-temperature structure.

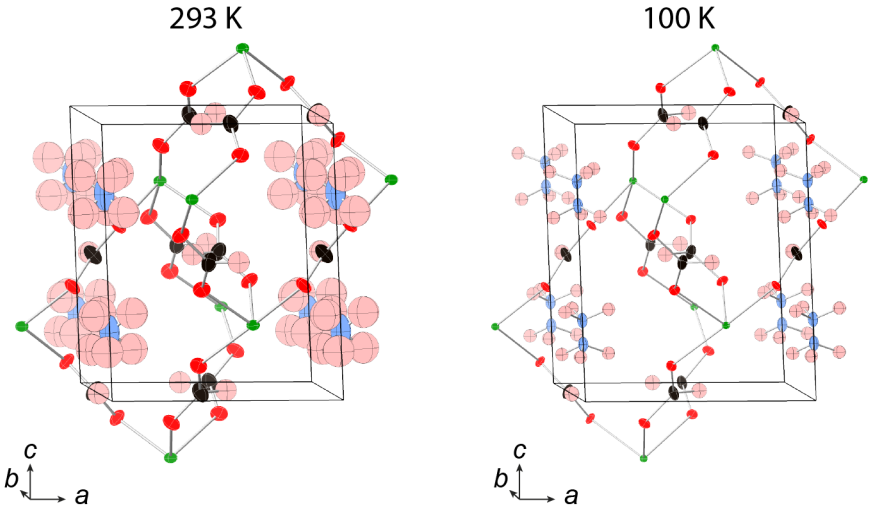

Figure S1: Crystal structures of $[NH_4][Ni(HCOO)_3]$ at 293 K and 100 K; thermal ellispoids are shown with 50% probability. The colours represent atom type where Ni is green, O is red, C is black, N is blue, and H is pink.

Table S1: Crystallographic details of $[NH_4][Ni(HCOO)_3]$ at ambient conditions and at 100 K.

	293 K	100 K
Formula	$C_3H_7N_1O_6Ni_1$	$C_3H_7N_1O_6Ni_1$
M_w	211.8	211.8
Crystal dimensions (μm)	100	100
Crystal System	Hexagonal	Hexagonal
Space Group	$P6_322$	$P6_322$
Z	2	2
a (Å)	7.28640(16)	7.26097(16)
c (Å)	8.05248(18)	8.0811(2)
V (Å^3)	370.242(19)	368.969(19)
Data collection		
No. of reflections		
measured	7581	7561
unique	361	361
unique with I > 2σ	330	351
R_{int}	0.0651	0.0412
Refinement		
No. of parameters	22	23
No. of restraints	1	1
R_1 [$I > 2\sigma(I)$]	0.0210	0.0176
wR_2 (all data)	0.0455	0.0467
$\Delta\rho_{max}/\Delta\rho_{min}$ (e^-Å^{-3})	0.19/−0.21	0.25/−0.46

2 HP-SCXRD of $[NH_4][Fe(HCOO)_3]$

The high-pressure single-crystal X-ray diffraction of $[NH_4][Fe(HCOO)_3]$ (**AFeF**) at 0.86 GPa showed that the monoclinic **AFeF**-II phase had formed [Fig. S2].

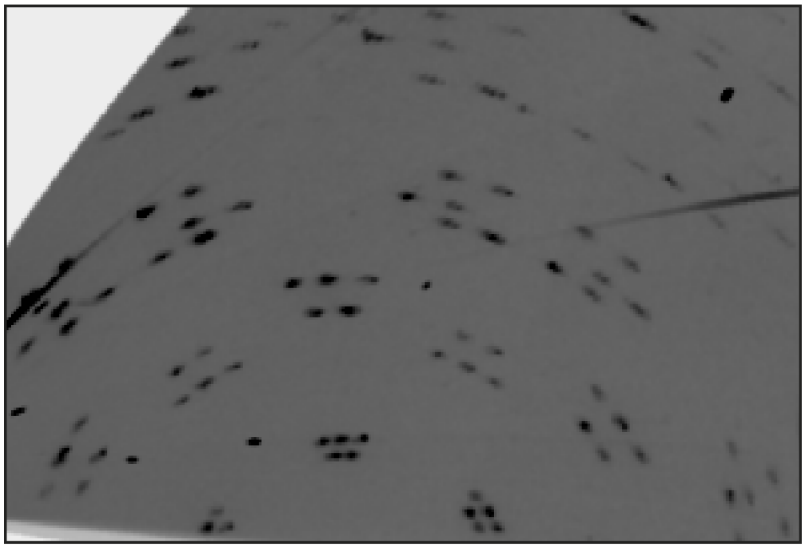

Figure S2: hk-5* reciprocal space reconstruction of **AFeF**-II at 0.86 GPa.

3 Twin matrices

The orientation matrix (UB) relates the indices h, k, l to a point in the diffraction pattern x, y, z by[S1]

$$\begin{bmatrix} x_1 \\ y_1 \\ z_1 \end{bmatrix} = \mathrm{UB}_1 \begin{bmatrix} h_1 \\ k_1 \\ l_1 \end{bmatrix}.$$

The h_2, k_2, l_2 indices of the second twin domain can be expressed as follows

$$\begin{bmatrix} h_2 \\ k_2 \\ l_2 \end{bmatrix} = \mathrm{UB}_2^{-1} \begin{bmatrix} x_1 \\ y_1 \\ z_1 \end{bmatrix} = \mathrm{UB}_2^{-1}\mathrm{UB}_1 \begin{bmatrix} h_1 \\ k_1 \\ l_1 \end{bmatrix}.$$

The twinning matrix (T) that relates the h, k, l indices from the first domain to the second domain is thus calculated by

$$\mathrm{T}_2 = \mathrm{UB}_2^{-1}\mathrm{UB}_1.$$

With reference to Figure 3 in the main text, the twin domains are related to each other as described by Table S2.

Table S2: Twin domain relations that are classified by the rotation of the unit cell along a specific axis.

Relation	rotation (°)	reciprocal axis
UB_1 and UB_2	180	[100]
UB_1 and UB_3	240	[010]
UB_3 and UB_4	180	[100]
UB_1 and UB_5	120	[010]
UB_5 and UB_6	180	[100]

Using the JANA software,[S2] the twinning matrices can be calculated by inputting the rotations which relate two twins as defined in Table S2. Another way to determine the same twinning matrices involves using the UB matrices of all six domains using the equations shown below. Note that these twinning matrices are based upon the following unit cell: $a = 6.668(6)$ Å, $b = 8.298(4)$ Å, $c = 7.393(6)$ Å, $\alpha = 90°$, $\beta = 116.64(11)°$, $\gamma = 90°$.

$$T_2 = UB_2^{-1}UB_1 = \begin{bmatrix} 1 & 0 & -2a\cos\beta/c \\ 0 & -1 & 0 \\ 0 & 0 & -1 \end{bmatrix} = \begin{bmatrix} 1 & 0 & 0.8088 \\ 0 & -1 & 0 \\ 0 & 0 & -1 \end{bmatrix}$$

$$T_3 = UB_3^{-1}UB_1 = \begin{bmatrix} -0.0656 & 0 & 0.8739 \\ 0 & 1 & 0 \\ -1.0742 & 0 & -0.9344 \end{bmatrix}$$

$$T_4 = UB_4^{-1}UB_1 = \begin{bmatrix} -0.9344 & 0 & 0.1182 \\ 0 & -1 & 0 \\ 1.0742 & 0 & 0.9344 \end{bmatrix}$$

which can also be derived from

$$T_4 = T_2 \times T_3 = \begin{bmatrix} 1 & 0 & 0.8088 \\ 0 & -1 & 0 \\ 0 & 0 & -1 \end{bmatrix} \times \begin{bmatrix} -0.0656 & 0 & 0.8739 \\ 0 & 1 & 0 \\ -1.0742 & 0 & -0.9344 \end{bmatrix} = \begin{bmatrix} -0.9344 & 0 & 0.1182 \\ 0 & -1 & 0 \\ 1.0742 & 0 & 0.9344 \end{bmatrix}$$

$$T_5 = UB_5^{-1}UB_1 = \begin{bmatrix} -0.9344 & 0 & -0.8739 \\ 0 & 1 & 0 \\ 1.0742 & 0 & -0.0656 \end{bmatrix}$$

$$T_6 = UB_6^{-1}UB_1 = \begin{bmatrix} -0.0656 & 0 & -0.9270 \\ 0 & -1 & 0 \\ -1.0742 & 0 & 0.0656 \end{bmatrix}$$

which can also be derived from

$$T_6 = T_2 \times T_5 = \begin{bmatrix} 1 & 0 & 0.8088 \\ 0 & -1 & 0 \\ 0 & 0 & -1 \end{bmatrix} \times \begin{bmatrix} -0.9344 & 0 & -0.8739 \\ 0 & 1 & 0 \\ 1.0742 & 0 & -0.0656 \end{bmatrix} = \begin{bmatrix} -0.0656 & 0 & -0.9270 \\ 0 & -1 & 0 \\ -1.0742 & 0 & 0.0656 \end{bmatrix}$$

If the twinning matrices and the UB matrix of the first domain are known, the UB matrices for the other five twins can be derived by the relation

$$\mathrm{UB}_2 = \mathrm{UB}_1\mathrm{T}_2^{-1}.$$

4 HP-SCXRD integration and refinements

Data integration of all six monoclinic twin domains of **AFeF**-II and **ANiF**-II were integrated individually using the software CrysAlisPro [Tables S3, S6, S8, S10].[S3] The JANA software[S2] was used to refine all six twin domains for each of the **AFeF**-II and **ANiF**-II data sets using the twin relationships defined in section 3 [Tables S4, S7, S9, S11].
The data from the six twin domains of **AFeF**-II was tested with the $C222_1$ space group in JANA, giving $R_1 = 0.152$, and wR_2 (all data) = 0.186. Space groups $C2$ and $P2_1/m$ were also tested, but no sensible structure solution could be determined or refined. When only the first two twin domains of **AFeF**-II are included in the structure refinement, the R values reduce to $R_1 = 0.082$, and wR_2 (all data) = 0.097 [Table S5].
Due to the coexistence of ambient and high-pressure phase peaks for the pressure points at 1.45 GPa and 1.8 GPa for **ANiF**-II (which for certain reflections overlap), refinement in JANA gave high R_1 values (up to 20%).
We note that due to the insufficient precision on the location of the nitrogen (that varied with subtle changes in the refinements), we could not reliably determine the polar displacements of the ammonium cation in the refined **ANiF**-II and **AFeF**-II structures (2.30 GPa and 0.86 GPa, respectively).

Table S3: Key parameters from each of the six data integrations belong to each of the twin domains in **AFeF**-II at 0.86 GPa.

	AFeF-II 0.86 GPa					
Empirical formula	$FeO_6C_3NH_7$					
space group	$P2_1$					
Z	2					
twin domain	1	2	3	4	5	6
a	6.670(4)	6.671(12)	6.664(9)	6.662(6)	6.670(2)	6.673(5)
b	8.296(2)	8.276(6)	8.296(4)	8.291(3)	8.314(2)	8.312(4)
c	7.401(2)	7.388(11)	7.393(8)	7.384(3)	7.403(4)	7.391(9)
β	116.74(5)	116.4(2)	116.40(17)	116.73(7)	116.81(5)	116.77(12)
V	365.7(3)	365.4(9)	366.1(7)	364.2(4)	366.4(2)	366.0(5)
Data collection						
No. of reflections	689	684	698	695	690	698
R_{int}	0.059	0.078	0.062	0.051	0.151	0.103

Table S4: Refinement parameters for **AFeF**-II with all 6 twin domains refined.

	AFeF-II 0.86 GPa
Refinement	
No. of reflections	4154
unique	3250
unique with I $> 3\sigma$	1549
No. of parameters	46
R_1 $[I > 3\sigma(I)]$	0.143
wR_2 (all data)	0.166
$\Delta\rho_{\max}/\Delta\rho_{\min}$ (e^-Å^{-3})	0.58, −0.44
Twin volume fractions	$V_I = 0.138(6)$
	$V_{II} = 0.141(2)$
	$V_{III} = 0.189(2)$
	$V_{IV} = 0.220(3)$
	$V_V = 0.176(3)$
	$V_{VI} = 0.136(3)$

Table S5: Refinement parameters for **AFeF**-II with the two first twin domains refined.

	AFeF-II 0.86 GPa
Refinement	
No. of reflections	1373
unique	1088
unique with I $> 3\sigma$	512
No. of parameters	42
R_1 $[I > 3\sigma(I)]$	0.082
wR_2 (all data)	0.097
$\Delta\rho_{\max}/\Delta\rho_{\min}$ (e^-Å^{-3})	0.44, −0.35
Twin volume fractions	$V_I = 0.1380(12)$
	$V_{II} = 0.1410(12)$
	$V_{III} = 0.189$
	$V_{IV} = 0.220$
	$V_V = 0.176$
	$V_{VI} = 0.136$

Table S6: Key parameters from each of the six data integrations belong to each of the twin domains in **ANiF**-II at 1.45 GPa.

	ANiF-II 1.45 GPa					
Empirical formula	$NiO_6C_3NH_7$					
space group	$P2_1$					
Z	2					
twin domain	1	2	3	4	5	6
a	6.727(15)	6.678(7)	6.701(6)	6.696(12)	6.723(7)	6.709(5)
b	8.0157(15)	8.0401(7)	8.0361(8)	8.0365(12)	8.0413(15)	8.0495(13)
c	7.280(7)	7.254(7)	7.244(8)	7.263(6)	7.218(15)	7.232(10)
β	117.87(19)	117.44(14)	117.59(14)	117.37(15)	117.48(19)	117.43(13)
V	347.0(8)	345.6(5)	345.7(5)	347.1(7)	346.2(8)	346.7(6)
Data collection						
No. of reflections	592	596	597	598	589	587
R_{int}	0.080	0.061	0.080	0.094	0.093	0.088

Table S7: Refinement parameters for **ANiF**-II at 1.45 GPa.

	ANiF-II 1.45 GPa
Refinement	
No. of reflections	3559
unique	2784
unique with I $> 3\sigma$	1237
No. of parameters	48
R_1 $[I > 3\sigma(I)]$	0.201
wR_2 (all data)	0.241
$\Delta\rho_{max}/\Delta\rho_{min}$ (e^-Å^{-3})	2.44, −1.57
Twin volume fractions	$V_I = 0.182(10)$
	$V_{II} = 0.173(3)$
	$V_{III} = 0.112(4)$
	$V_{IV} = 0.127(4)$
	$V_V = 0.201(5)$
	$V_{VI} = 0.205(5)$

Table S8: Key parameters from each of the six data integrations belong to each of the twin domains in **ANiF**-II at 1.8 GPa.

	ANiF-II 1.8 GPa					
Empirical formula	$NiO_6C_3NH_7$					
space group	$P2_1$					
Z	2					
twin domain	1	2	3	4	5	6
a	6.521(10)	6.527(8)	6.59(3)	6.517(11)	6.510(9)	6.551(12)
b	8.0567(12)	8.0609(10)	8.052(2)	8.0618(10)	8.0540(17)	8.056(2)
c	7.275(5)	7.253(11)	7.24(3)	7.281(5)	7.26(3)	7.25(3)
β	116.68(14)	116.73(18)	116.8(5)	116.63(14)	116.5(3)	116.7(3)
V	341.5(6)	340.8(7)	343(2)	341.9(6)	341(2)	342(1)
Data collection						
No. of reflections	584	592	602	590	583	591
R_{int}	0.0592	0.0778	0.1009	0.0762	0.1415	0.0715

Table S9: Refinement parameters for **ANiF**-II at 1.8 GPa.

	ANiF-II 1.8 GPa
Refinement	
No. of reflections	3522
unique	2392
unique with $I > 3\sigma$	837
No. of parameters	48
R_1 $[I > 3\sigma(I)]$	0.164
wR_2 (all data)	0.221
$\Delta\rho_{max}/\Delta\rho_{min}$ (e^-Å^{-3})	2.81, −1.34
Twin volume fractions	V_I = 0.201(12)
	V_{II} = 0.189(4)
	V_{III} = 0.117(4)
	V_{IV} = 0.140(4)
	V_V = 0.209(9)
	V_{VI} = 0.144(5)

Table S10: Key parameters from each of the six data integrations belong to each of the twin domains in **ANiF**-II at 2.3 GPa.

	ANiF 2.3 GPa					
Empirical formula	$NiO_6C_3NH_7$					
space group	$P2_1$					
Z	2					
twin domain	1	2	3	4	5	6
a	6.310(12)	6.310(17)	6.300(19)	6.25(2)	6.325(4)	6.341(5)
b	8.0602(10)	8.0549(16)	8.053(2)	8.0910(15)	8.0534(10)	8.0470(11)
c	7.269(5)	7.26(2)	7.26(2)	7.271(8)	7.214(14)	7.225(13)
β	115.66(15)	115.6(4)	115.6(4)	115.4(2)	115.53(14)	115.69(14)
V	333.2(7)	333(1)	332(1)	332(1)	331.6(7)	332.2(6)
Data collection						
No. of reflections	568	569	568	575	560	561
R_{int}	0.125	0.123	0.102	0.083	0.078	0.074

Table S11: Refinement parameters for **ANiF**-II.

	ANiF-II 2.3 GPa
Refinement	
No. of reflections	3401
unique	2542
unique with $I > 3\sigma$	1110
No. of parameters	46
R_1 $[I > 3\sigma(I)]$	0.111
wR_2 (all data)	0.142
$\Delta\rho_{max}/\Delta\rho_{min}$ (e^-Å^{-3})	1.00, −0.93
Twin volume fractions	$V_I = 0.176(6)$
	$V_{II} = 0.202(3)$
	$V_{III} = 0.144(2)$
	$V_{IV} = 0.141(2)$
	$V_V = 0.174(3)$
	$V_{VI} = 0.163(3)$

5 Framework angle pressure-dependence

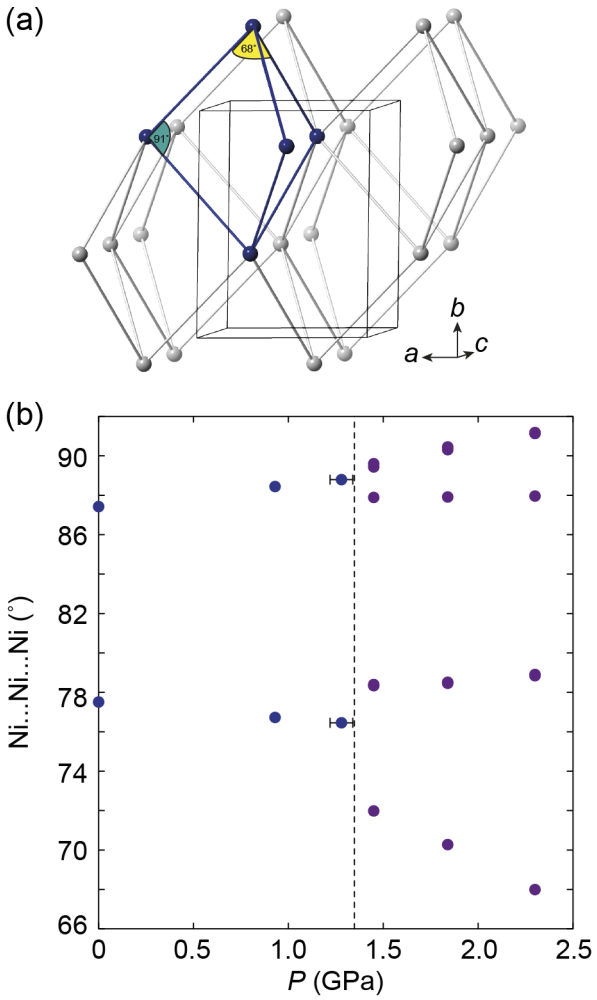

Figure S3: (a) Framework connectivity and geometry of **ANiF**-II at 2.3 GPa where rods indicate the Ni-formate-Ni bonding for simplicity. The two Ni···Ni···Ni framework angles which are found to vary most upon compression are highlighted. These angle variations are responsible for distorting the hexagon motifs in the **ac**-plane. (b) The pressure dependence of the Ni···Ni···Ni framework angles.

6 Rietveld neutron powder diffraction fits of AZnF

Rietveld refinements of the high-resolution neutron powder diffraction of **AZnF** on GEM at ISIS confirmed the presence of hydrogen on the ammonium deuterium positions. Figure S4 shows that the best fits are obtained for a model with no H or D positions on the ammonium cation, or with refined occupancies of H and D that come close to a cancellation of the scattering intensity of this site due to the scattering lengths of H (−3.739 fm) and D (+6.671 fm).

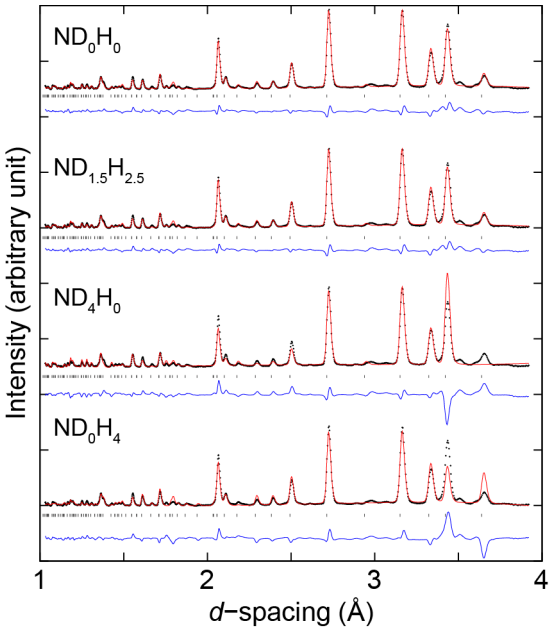

Figure S4: Rietveld fits of neutron powder diffraction of **AZnF** at ambient conditions with different occupancies for the H or D positions of the ammonium cation. Experimental data are given as points, the fitted profile as a solid red line, and the difference (data–fit) as a blue line. The *hkl* tick marks in grey represent the $P6_322$ **AZnF** model.

Rietveld refinements of **AZnF** were performed on all variable-pressure neutron powder diffraction patterns. Distance and angle restraints were used on the formate ligands, as well as distance restraints between the oxygen of the formate and the zinc to maintain sensible geometry of the formate and of the zinc coordination sphere, respectively. Figures S5 and S6 show the fits to the ambient $P6_322$ and high-pressure $P2_1$ phases upon compression, respectively, while Figure S7 shows the fits upon decompression.

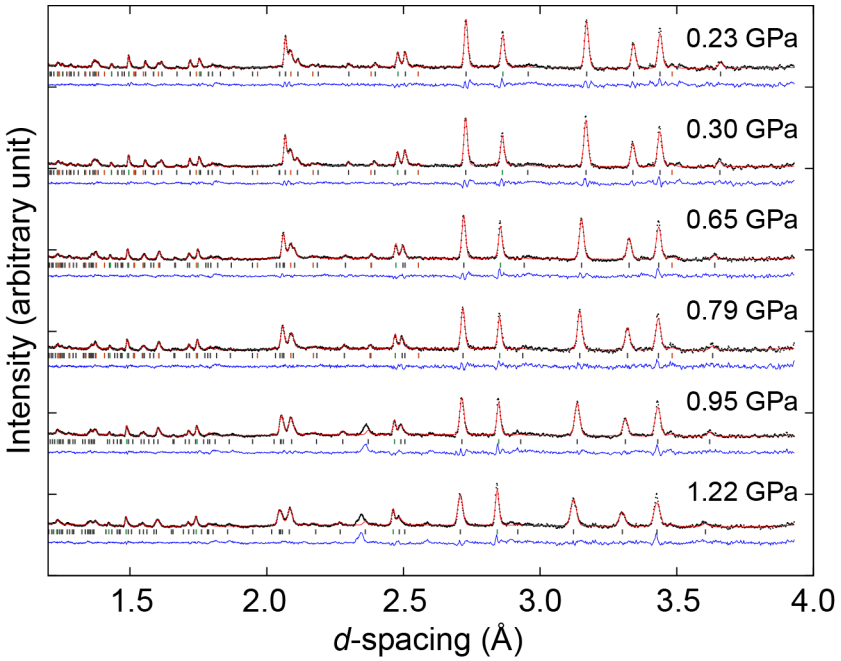

Figure S5: Rietveld fits of the variable-pressure neutron powder diffraction of **AZnF** from 0–1.22 GPa. Experimental data are given as points, the fitted profile as a solid red line, and the difference (data–fit) as a blue line. The *hkl* tick marks in grey, green, and orange represent the $P6_322$ **AZnF** model, lead, and Alumina, respectively.

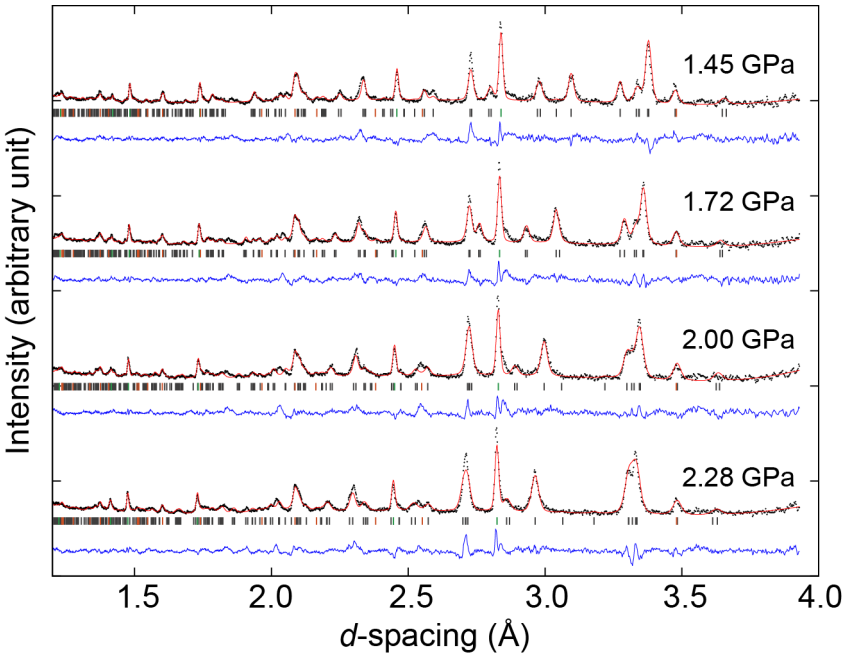

Figure S6: Rietveld fits of the variable-pressure neutron powder diffraction of **AZnF**-II from 1.45–2.28 GPa. Experimental data are given as points, the fitted profile as a solid red line, and the difference (data–fit) as a blue line. The *hkl* tick marks in grey, green, and orange represent the $P2_1$ **AZnF**-II model, lead, and Alumina, respectively.

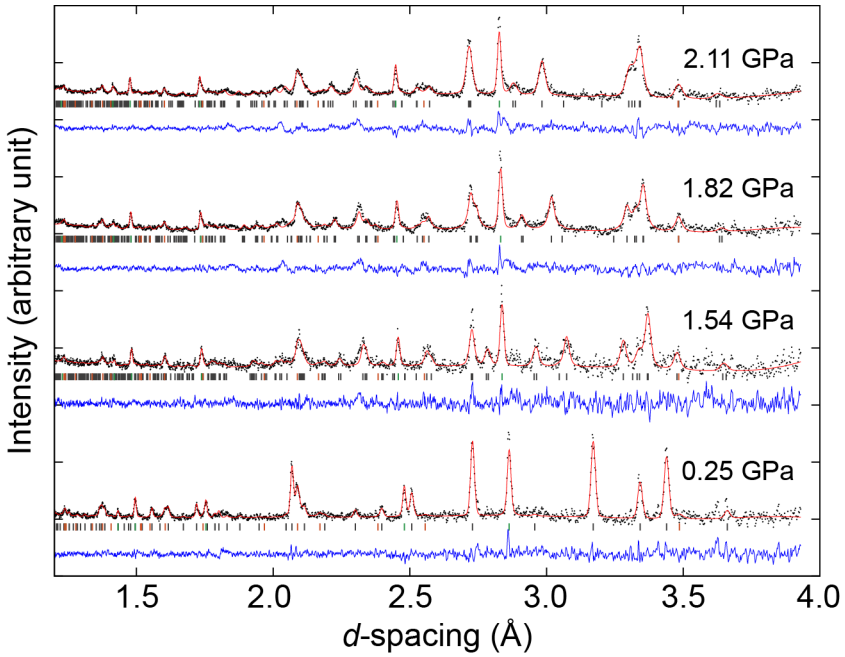

Figure S7: Rietveld fits of the variable-pressure neutron powder diffraction of **AZnF**-II upon decompression. Experimental data are given as points, the fitted profile as a solid red line, and the difference (data–fit) as a blue line. The *hkl* tick marks in grey, green, and orange represent the **AZnF**-II or **AZnF** models, lead, and Alumina, respectively.

7 Variable-pressure lattice parameters for AZnF

Table S12: Pressure-dependent lattice parameters for **AZnF** determined from Rietveld refinements of the neutron diffraction data. The asterisks indicate data upon decompression.

run no.	P (GPa)	a (Å)	c (Å)	V (Å^3)
76574-76577	0.22(2)	7.2932(3)	8.1578(7)	375.78(5)
76583-76587	0.23(2)	7.2932(3)	8.1565(6)	375.72(4)
76588-76592	0.30(2)	7.2877(3)	8.1560(6)	375.14(4)
76598-76602	0.65(2)	7.2509(3)	8.1591(6)	371.50(4)
76603-76605	0.79(2)	7.2355(4)	8.1611(8)	370.01(5)
76606-76610	0.95(2)	7.2143(5)	8.1660(9)	368.06(6)
76611-76615	1.22(2)	7.1832(6)	8.1704(12)	365.10(8)
76644	0.63(2)*	7.2498(10)	8.161(2)	371.45(14)
76645-76646	0.25(2)*	7.2945(6)	8.1550(11)	375.98(8)

Table S13: Pressure-dependent lattice parameters for **AZnF**-II determined from Rietveld refinements of the neutron diffraction data. The asterisks indicate data upon decompression.

run no.	P (GPa)	a (Å)	b (Å)	c (Å)	β (°)	V (Å^3)
76616-76620	1.45(2)	6.6594(10)	8.1702(12)	7.3118(11)	116.85(2)	354.94(11)
76621-76625	1.72(2)	6.5228(9)	8.1659(13)	7.3139(14)	116.34(2)	349.14(12)
76626-76630	2.00(3)	6.4132(11)	8.1732(16)	7.3232(14)	116.17(2)	344.49(12)
76631-76636	2.28(3)	6.3327(10)	8.1672(18)	7.3197(15)	115.91(2)	340.52(13)
76637-76639	2.11(3)*	6.3807(11)	8.1716(18)	7.3206(18)	116.05(2)	342.91(14)
76640-76641	1.82(3)*	6.4660(13)	8.1754(20)	7.3232(22)	116.33(3)	346.95(18)
76643	1.54(3)*	6.6048(18)	8.1683(23)	7.3127(23)	116.64(3)	352.66(20)

8 2nd-order B-M EOS fit to AMF phases

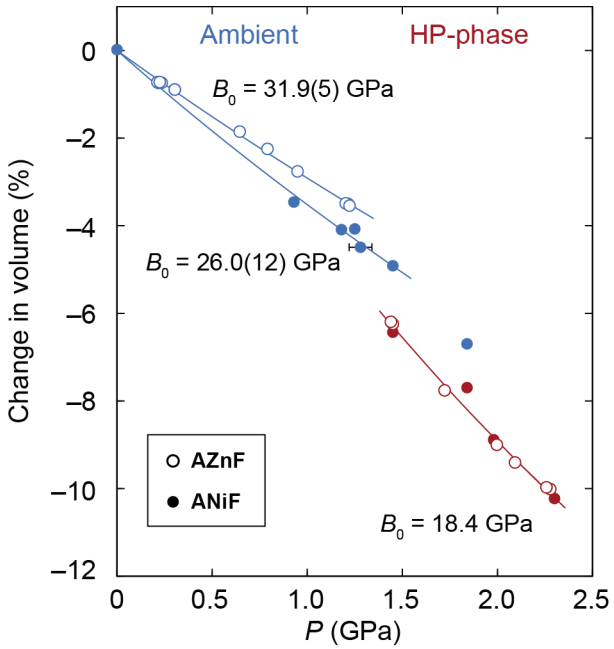

Figure S8: The relative changes in the unit-cell volume of the ambient (blue) and high-pressure phases (red) of **ANiF** (filled circles) and **AZnF** (empty circles). Second-order B-M EOS are fitted to ambient **ANiF** and **AZnF** phases using PASCal,[S4] and a modified version of the second-order B-M EOS to the **AZnF**-II phase as detailed in Ref. S5.

9 Crystallographic details for AZnF

Table S14: Crystallographic details determined by neutron powder diffraction for **AZnF** at 0.22(2) GPa.

Space Group	$P6_322$			
a (Å)	7.2932(3)			
c (Å)	8.1578(7)			
V (Å^3)	375.78(5)			
Z	2			
wR$_p$	4.153			
Atom	x	y	z	U_{iso} (Å^2)
Zn1	$\frac{2}{3}$	$\frac{1}{3}$	0.75	0.079(10)
N1	0	0	0.75	0.052(5)
O1	0.8906(9)	0.3109(7)	0.9027(10)	0.026(2)
C1	0	0.4409(9)	0	0.090(6)
D1	0	0.580(2)	0	0.122(6)

Table S15: Crystallographic details determined by neutron powder diffraction for **AZnF** at 1.22(2) GPa.

Space Group	$P6_322$			
a (Å)	7.1832(6)			
c (Å)	8.1704(12)			
V (Å^3)	365.10(8)			
Z	2			
wR$_p$	4.509			
Atom	x	y	z	U_{iso} (Å^2)
Zn1	$\frac{2}{3}$	$\frac{1}{3}$	0.75	0.085(12)
N1	0	0	0.75	0.060(6)
O1	0.8839(10)	0.3047(8)	0.9010(10)	0.028(2)
C1	0	0.4432(11)	0	0.078(6)
D1	0	0.587(3)	0	0.161(9)

Table S16: Crystallographic details determined by neutron powder diffraction for **AZnF**-II at 1.45(2) GPa.

Space Group	$P2_1$			
a (Å)	6.6594(10)			
b (Å)	8.1702(12)			
c (Å)	7.3118(11)			
β (°)	116.85(2)			
V (Å^3)	354.94(11)			
Z	2			
wR$_p$	4.185			
Atom	x	y	z	U_{iso} (Å^2)
Zn1	0.683(4)	0.25	0.334(3)	0.061(2)
N1	−0.103(4)	0.202(4)	−0.103(4)	0.039(10)
O1	0.307(3)	0.918(2)	0.898(4)	0.026(4)
O2	0.905(4)	0.409(3)	0.563(3)	0.026(4)
O3	0.523(4)	0.924(3)	0.645(4)	0.026(4)
O4	0.734(4)	0.066(4)	0.543(3)	0.026(4)
O5	0.539(4)	0.646(4)	0.943(5)	0.026(4)
O6	0.955(4)	0.141(2)	0.294(2)	0.026(4)
C1	0.049(3)	0.050(2)	0.448(2)	0.120(13)
C2	0.391(3)	0.441(2)	0.467(2)	0.120(13)
C3	0.473(2)	0.010(2)	0.014(3)	0.120(13)
D1	0.016(4)	0.080(3)	0.585(2)	0.114(13)
D2	0.483(3)	0.384(3)	0.621(2)	0.114(13)
D3	0.646(3)	−0.045(2)	0.095(5)	0.114(13)

Table S17: Crystallographic details determined by neutron powder diffraction for **AZnF**-II at 2.28(3) GPa.

Space Group	$P2_1$			
a (Å)	6.3327(10)			
b (Å)	8.1672(18)			
c (Å)	7.3197(15)			
β (°)	115.91(2)			
V (Å^3)	340.52(13)			
Z	2			
wR$_p$	4.711			
Atom	x	y	z	U_{iso} (Å^2)
Zn1	0.668(3)	0.25	0.308(2)	0.090(16)
N1	−0.084(6)	0.243(4)	−0.064(5)	0.072(9)
O1	0.250(2)	0.9368(8)	0.847(3)	0.014(3)
O2	0.917(2)	0.376(2)	0.5899(6)	0.014(3)
O3	0.541(3)	0.9286(8)	0.657(2)	0.014(3)
O4	0.732(2)	0.0831(9)	0.5104(5)	0.014(3)
O5	0.5491(7)	0.627(2)	0.959(2)	0.014(3)
O6	0.949(3)	0.1342(7)	0.2860(11)	0.014(3)
C1	0.065(2)	0.0258(5)	0.4376(4)	0.043(7)
C2	0.3502(10)	0.4519(4)	0.4697(4)	0.043(7)
C3	0.4307(6)	−0.0076(5)	−0.0175(10)	0.043(7)
D1	0.063(5)	0.0680(7)	0.6069(16)	0.128(13)
D2	0.469(2)	0.3661(8)	0.6365(9)	0.128(13)
D3	0.560(2)	−0.0895(6)	0.0452(16)	0.128(13)

10 N···O distances in AZnF

The N···O distances were evaluated as a function of pressure, and the average of the closest six N···O distances (divided into the average of the four shortest, and the average of the two longest) are shown in Figure S9. In addition to the observed pressure-dependent N···O distances, two additional hypothetical pressure-dependent N···O distances were calculated based upon (*i*) a non-polar position of the N, and (*ii*) a position of N that would give a polarisation of $4\,\mu\mathrm{C\,cm^{-1}}$, thus maintaining the polarisation value observed at 1.45 GPa up to 2.28 GPa. Both hypothetical N positions would only vary in the y-coordinate, the x- and z- coordinates take the original values of the observed N position. The evolutions of these three N···O distances (one observed, two hypothetical) show that a non-polar arrangement of the N atoms gives rise to larger distances for the two long N···O distances. Thus a polar arrangement is favoured due to the closer interactions of the ammonium cation to the six neighbouring oxygen atoms of the formate linkers. If the polarity observed at 1.45 GPa ($4\,\mu\mathrm{C\,cm^{-1}}$) is maintained with increasing pressure, the N···O distances would become even closer, which would suggest greater interactions with the six neighbouring oxygens. However, we observe that the structure evolves to exhibit lower polarisation with increasing pressure. This is related to the competing effect of the packing of the structure, and is described in Section 11.

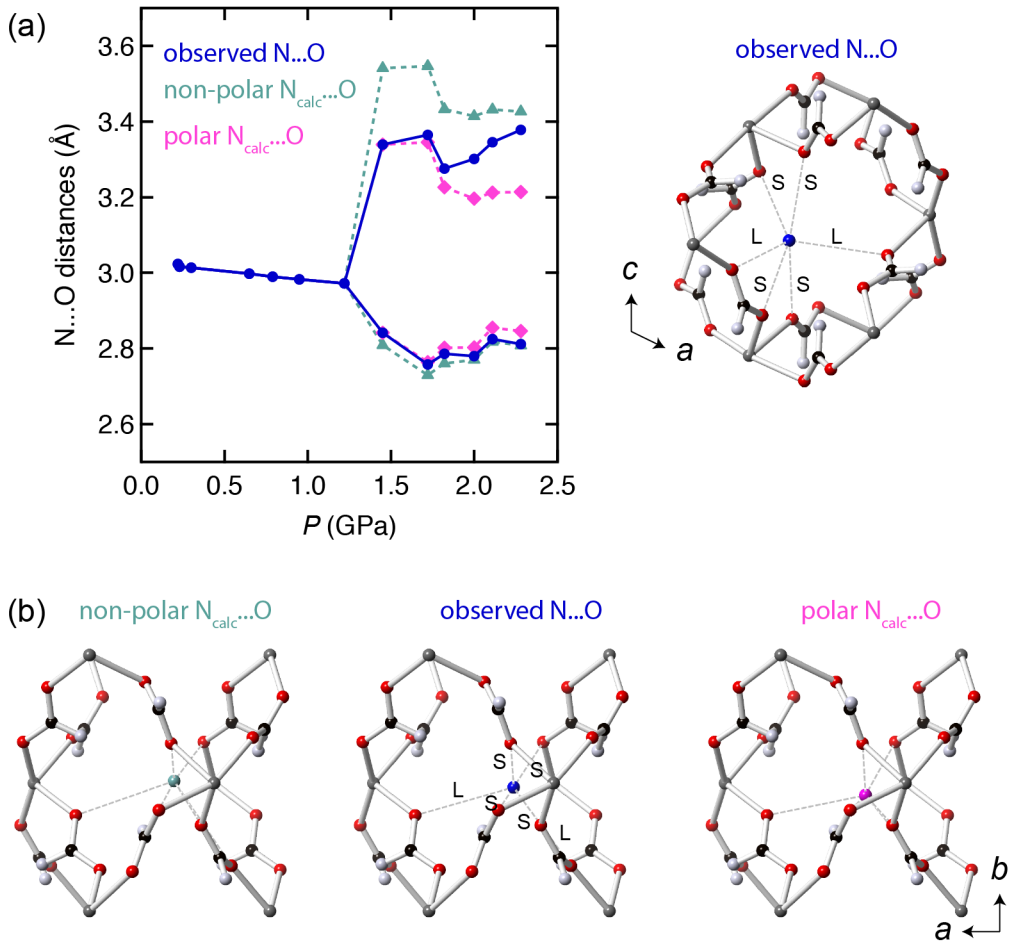

Figure S9: (a) The average of the four shortest and two longest N$\cdots$O distances (of the closest six) shown for N$\cdots$O distances as observed (blue circles), with a non-polar position of the N (green triangles), and with the polarisation of $\sim$4 μC cm^{-1} maintained (pink diamonds) as a function of pressure. The structural model on the right indicates the short (S) and long (L) N$\cdots$O distances. (b) The structural models at 2.0 GPa for the three N positions. Note that the N y-coordinate is the only parameter that is changed for the two hypothetical non-polar and polar at 4 μC cm^{-1} cases.

11 Void maps of the zinc formate

Void maps were calculated for **AZnF** using the software Olex2[S6] as a function of pressure with the nitrogen atom removed from the structure (no voids would be observed when the ammonium cation is within the crystal structure) [Figure S10]. This was performed to highlight how the space near the position of the ammonium cation varies with pressure. We observe that as pressure is increased, the available space for the ammonium cation to reside in reduces in size and shifts towards the non-polar position.

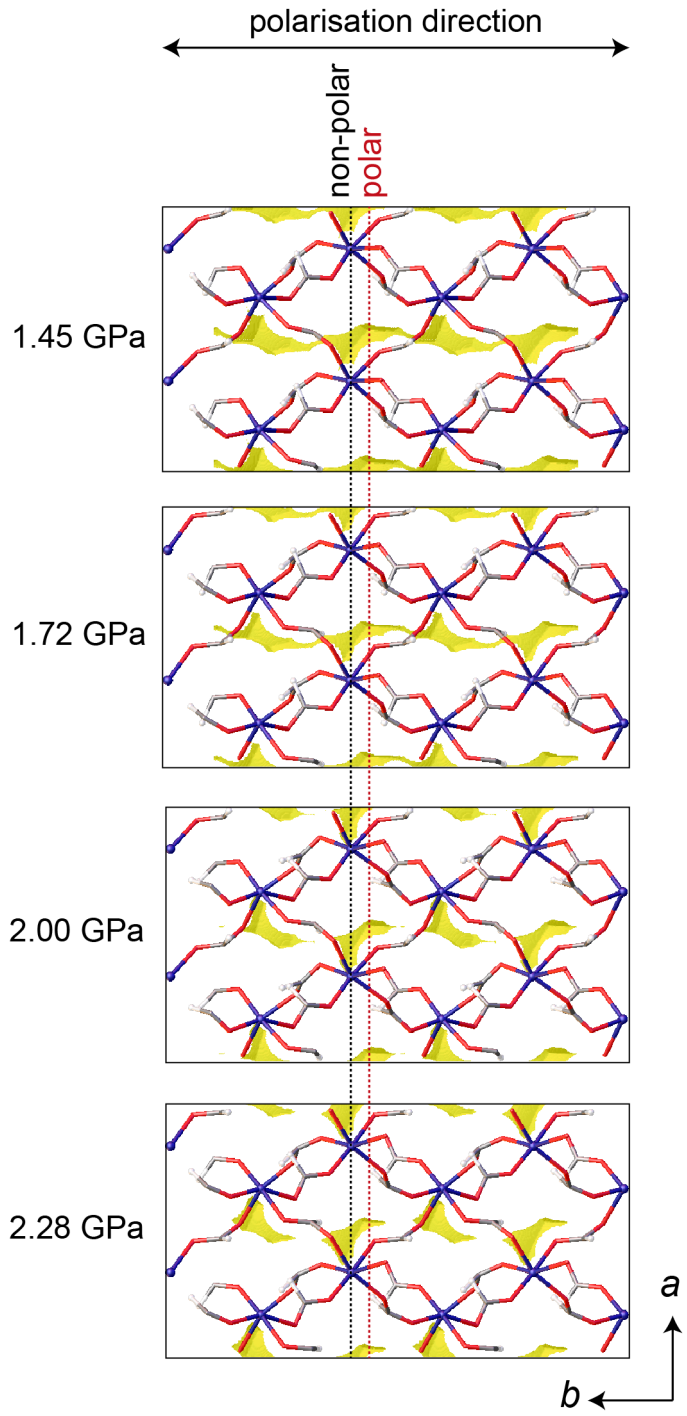

Figure S10: Void maps in yellow of zinc formate (the nitrogen atom is removed from the structure) as a function of pressure. The void maps represent a distance of 1.1 Å from the framework atoms (with a resolution of 0.05 Å). The non-polar and polar positions of the nitrogen atom along the *b*-axis are indicated by the dotted black and red lines, respectively.

12 HP Raman spectroscopy

High-pressure Raman scattering experiments were performed using Dilor XY and a LabRam Spectrometer (resolution 2 cm^{-1}), equipped with a He-Ne laser source with the excitation wavelength of 632.8 nm. The laser power in the range of 300–500mW was used for measurements. The pressure was measured by ruby fluorescence, and Raman spectra were collected on **ANiF** and **AFeF** single crystals up to 3.5 GPa (Ar as PTM) within a diamond-anvil cell [Figure S11]. The suggested assignment of the Raman peaks is based upon the works from Refs. S7 and S8. The peaks which exhibit splitting upon the high-pressure phase transition of the **ANiF** and **AFeF** compounds belong to the vibrational modes of the formate linker, which agrees with the refined $P2_1$ structural models consisting of a distorted metal formate structure and a previous high-pressure Raman study of $[ND_4][Zn(DCOO)_3]$.[S9]

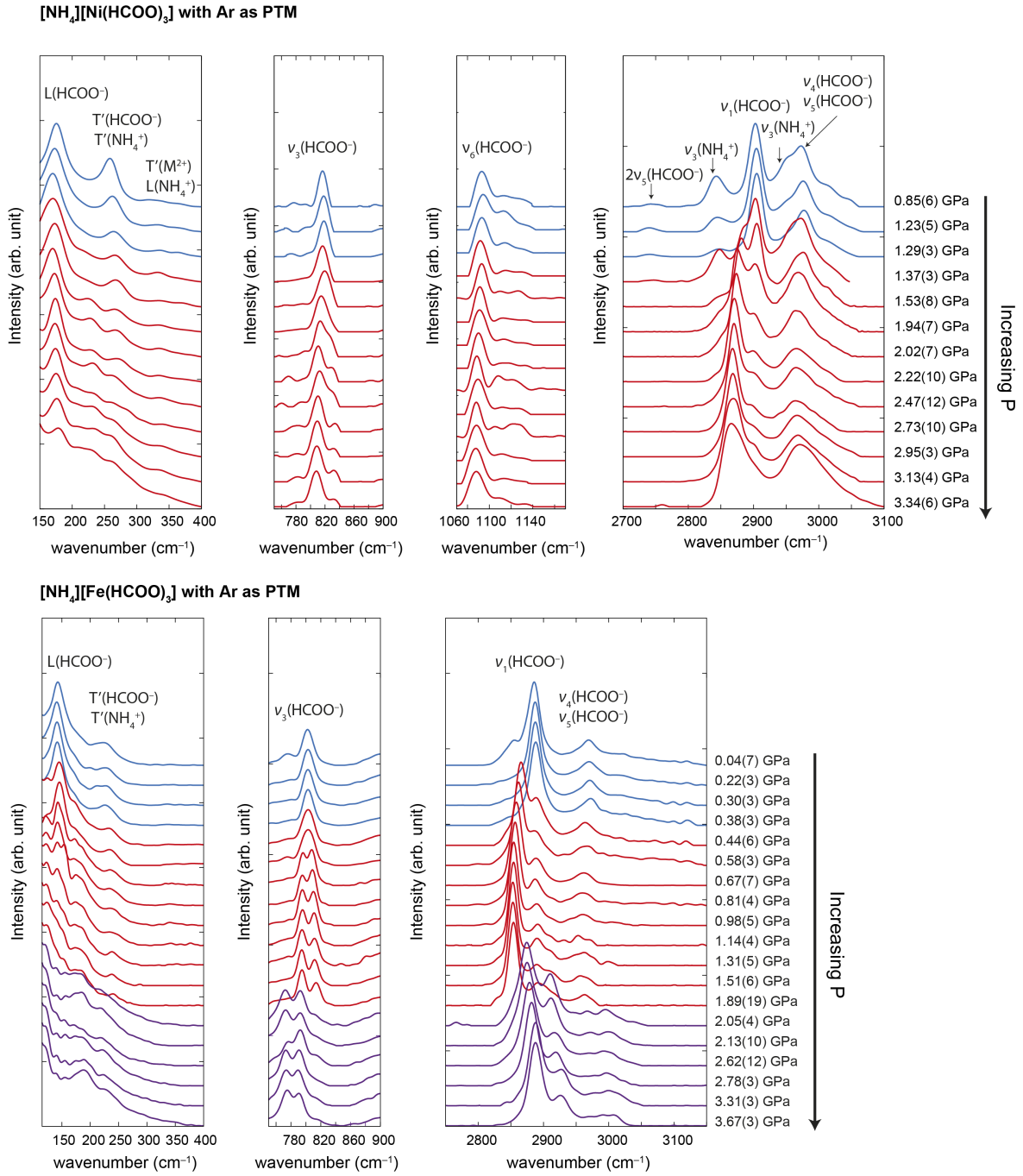

Figure S11: Pressure-dependent Raman spectra for **ANiF** and **AFeF** crystals loaded with argon as the PTM. Background removal and smoothing of the Raman spectra were applied. (From I. E. Collings, E. Bykova, M. Bykov, S. Petitgirard, M. Hanfland, D. Paliwoda, L. Dubrovinsky, N. Dubrovinskaia, *ChemPhysChem*, 2016, DOI: 10.1002/cphc.201600854. Copyright Wiley-VCH Verlag GmbH & Co. KGaA. Figure reproduced with permission.)

References

(S1) *International Tables for Crystallography Volume C*, edited by A. J. C. Wilson, E. Prince (Kluwer Academic Publishers, 1999), page 532.

(S2) V. Petříček, M. Dušek, L. Palatinus, *Z. Kristallogr.* **2014**, 229, 345–352.

(S3) Agilent Technologies, CrysAlisPro Software system, 2013.

(S4) M. J. Cliffe, A. L. Goodwin, *J. Appl. Cryst.* **2012**, 45, 1321–1329.

(S5) N. Sata, G. Shen, M. L. Rivers, S. R. Sutton, *Phys. Rev. B* **2002**, 65, 104114.

(S6) O. V. Dolomanov, L. J. Bourhis, R. J. Gildea, J. A. K. Howard, H. Puschmann, *J. Appl. Cryst.* **2009**, 42, 339–341.

(S7) M. Mączka, A. Pietraszko, B. Macalik, K. Hermanowicz, *Inorg. Chem.* **2014**, 53, 787-794.

(S8) M. Mączka, K. Szymborska-Małek, A. Ciupa, J. Hanuza, *Vib. Spectrosc.* **2015**, 77, 17–24.

(S9) M. Mączka, P. Kadłubański, P. T. C. Freire, B. Macalik, W. Paraguassu, K. Hermanowicz, J. Hanuza, *Inorg. Chem.* **2014**, 53, 9615–9624.